J. Phys. D: Appl. Phys. **42** (2009) 225505 (9pp) doi:10.1088/0022-3727/42/22/225505

Capillarity and dielectrophoresis of liquid deuterium

T B Jones[1,4], R Gram[2], K Kentch[3] and D R Harding[2]

[1] Department of Electrical and Computer Engineering, University of Rochester, Rochester, NY 14627, USA
[2] Laboratory for Laser Energetics, University of Rochester, Rochester, NY 14627, USA
[3] Department of Biomedical Engineering, University of Rochester, Rochester, NY 14627, USA

E-mail: jones@ece.rochester.edu

Received 23 June 2009, in final form 7 October 2009
Published 6 November 2009
Online at stacks.iop.org/JPhysD/42/225505

Abstract
The ponderomotive force, exerted upon all dielectric liquids by a non-uniform electric field, can be used for the remote, voltage-controlled manipulation of 10 to 100 μL volumes of cryogenic liquids. This liquid dielectrophoretic (DEP) effect, imposed by specially designed electrodes, combines with capillarity to influence the hydrostatic equilibria of liquid deuterium. A simple, one-dimensional model accurately predicts the measured meniscus rise of D_2 against gravity for sufficiently wide, parallel electrodes. For narrow electrodes, where the sidewalls influence the equilibrium, a finite element solution using the Surface Evolver software correctly describes the shape of the meniscus. A bifurcation phenomenon previously observed for room temperature dielectrics is also observed in liquid deuterium. Cryo-DEP actuation has potential applications ranging from metering precise volumes of liquid deuterium for laser target fuelling to manipulation of liquid nitrogen for cryo-preservation of biological samples.

(Some figures in this article are in colour only in the electronic version)

1. Introduction

Liquid dielectrophoresis (DEP) enlists the so-called ponderomotive force, which selectively attracts dielectric liquids with relatively higher dielectric constant into regions where the imposed electric field is stronger. Fluids with relatively lower dielectric constant, including vapour and gas, are simultaneously repelled from strong electric field regions. The critical requirement for DEP liquid management is the non-uniformity of the electric field imposed by the particular design of the electrodes. The dielectric nature of cryogenic liquids means that these substances exhibit dielectrophoresis, and in fact, liquid DEP offers some advantages as a means to move and manipulate them remotely without resort to mechanical pumps or other complex apparatus. Furthermore, their very low electrical conductivity means that Joule heating is of no consequence. As a result, DEP manipulation of cryogenic liquids is relatively easy to exploit using properly designed electrodes and easy to control via voltage modulation.

In the early years of the space programme, liquid DEP was seriously considered as a means to manage cryo-propellants in zero gravity [1]. Low gravity experiments with cryogenic nitrogen have been reported more recently [2]. In this paper, we report experiments with a simple, parallel plate geometry intended to investigate the basic capillary and DEP force coupled hydrostatics of liquid D_2 in the temperature range from ~19 to ~27 K. A simple hydrostatic model adequately describes the effectively additive natures of the capillary and DEP forces upon the net height of rise against gravity. We further demonstrate a bifurcation effect that might ultimately be exploited in the dispensing and metering of small cryo-liquid volumes.

2. Motivation

The motivation for this work stems from the need to accelerate and ultimately to automate the fabrication of the precision cryogenic targets used in laser-driven inertial confinement fusion experiments. These targets are typically concentric shells ~1 mm in diameter with ~100 μm thick walls of

[4] Author to whom any correspondence should be addressed.

cryogenic deuterium and tritium (DT) ice [3]. The interior of the shells contains more DT, but in liquid form. Future, more powerful laser drivers, such as the National Ignition Facility now nearing completion at the Lawrence Livermore National Laboratory in California (USA), will use targets up to ~4.7 mm in diameter with ~350 μm thick walls [4]. These targets are formed from low-density polymer foam shells that serve as mandrels for the final DT ice structures. The current technique of making them is a batch process that takes as long as two weeks [5]. Given the sizeable tritium content (>15Ci for large targets) and the fact that a ~1 GW fusion-powered electric power plant will consume > 500 000 of these targets per day [6], the present production method must be replaced because it ties up a huge inventory of highly radioactive tritium. A fully automated, just-in-time fabrication technology requiring no human intervention, possibly based on microfluidics, is needed [7]. The present fuelling process, where liquid DT is loaded into the fragile shells, involves permeating gaseous hydrogen through an outer membrane by slowly ramping up the pressure to ~1000 bars [8]. This process is far too slow and cumbersome, so our goal is to develop automated means to manipulate liquid hydrogen for the fuelling operation.

Another interesting application for electric field mediated cryo-microfluidics is envisioned in the emerging field of cryo-preservation, that is the long-term storage of human tissue and biological particles at low temperature for later use in therapeutic treatments. The barrier to a practical technology of cryo-preservation is the shear number of samples that have to be preserved and the difficulties associated with proper freezing and thawing of cells without their incurring damage [9]. The capabilities of liquid DEP to dispense, move and manipulate small volumes of liquid nitrogen might prove very useful in this field.

3. Nature of cryogenic hydrogen

The critical properties of the isotopes of cryogenic hydrogen—H_2, D_2 and T_2—have been intensively studied. There are many published measurements as well as some crucial extrapolations intended to fill gaps in the measured data [10]. One may anticipate the liquid DEP behaviour of cryogenic liquid hydrogen to be unique based on its physical properties. For example, compared with room temperature liquids, cryogenic deuterium has very low density ($\rho \approx 0.18\,\mathrm{gm\,cm^{-3}}$), dielectric constant ($\kappa \approx 1.25$) and surface tension ($\gamma \approx 0.0038\,\mathrm{N\,m^{-1}}$). Also, the liquid maintains zero contact angle against almost all solid materials [11]. Further, the useable range of temperatures and (saturated vapour) pressures spans conditions from the triple point ($T = 18.7\,\mathrm{K}$, $p = 17\,\mathrm{kPa}$) almost to the critical point ($T = 38\,\mathrm{K}$, $p = 1.7\,\mathrm{MPa}$), the consequence being rather strong temperature dependences for some of the important fluid properties. Low viscosity creates still another distinction of likely importance in the dynamics of target fuelling, though this issue is not addressed in this paper. For ~10 to ~100 μL D_2 droplets, the size range appropriate for laser targets, the capillary force is significant, but the liquid DEP force can be made comparable or dominant if due care is taken to avoid electric breakdown. The experiments reported here are limited to deuterium, which is easy to handle and an excellent insulator. Tritium, a radioactive isotope, is a different matter. With abundant β particles produced in its bulk, liquid T_2 may very well behave like a conductive liquid. Some speculation on the effect of such bulk charge transport on electric field mediated microfluidics is offered in section 8 of the paper.

4. Theory

The capillary rise of a liquid covered by a gas or a vapour of negligible density between two parallel and vertical plates is h_{cap} [12]

$$h_{\mathrm{cap}} \approx 2\gamma \cos\theta_{\mathrm{c}}/(\rho_{\mathrm{l}} - \rho_{\mathrm{v}})\, gd, \tag{1}$$

where γ is the surface tension, ρ_l and ρ_{v} are the liquid and vapour mass densities, θ_{c} is the contact angle, d is the plate spacing and $g = 9.81\,\mathrm{m\,s^{-2}}$ is the terrestrial acceleration due to gravity. Usually, $\rho_{\mathrm{l}} \gg \rho_{\mathrm{v}}$. The experimental geometry is illustrated in figure 1(*a*). Equation (1) assumes that $h_{\mathrm{cap}} \gg d$, and further that the plates are wide compared with their spacing, that is $w \gg d$. The Bond number *Bo* is a useful dimensionless modulus that may be extracted from equation (1):

$$Bo \equiv h_{\mathrm{cap}}/d = 2\gamma \cos\theta_{\mathrm{c}}/(\rho_{\mathrm{l}} - \rho_{\mathrm{v}})\, gd^2. \tag{2}$$

Bo measures the relative importance of surface tension and gravity. For the well-known case of a sessile droplet resting on a flat, horizontal surface, one replaces plate spacing d in equation (1) by droplet radius R. Then, the magnitude of *Bo* determines whether the droplet takes the shape of a spherical cap ($Bo \gg 1$) or a flattened disc ($Bo \ll 1$). In the parallel plate experiment of interest to us, the transverse profile of the liquid meniscus between the plates assumes the shape of a semi-circular arc for large Bond number.

If the liquid is a dielectric, the plates are conductive electrodes, and voltage V is applied between them, the ponderomotive (DEP) effect exerts an additional upward force on the liquid column. Refer again to figure 1(*a*). Pellat studied this behaviour in 1895 [13]. Assuming, as before, that the plates are very wide compared with the spacing, the dielectric height of rise is [14]

$$h_{\mathrm{DEP}} \approx (\kappa_{\mathrm{l}} - \kappa_{\mathrm{v}})\, \varepsilon_{\mathrm{o}} V^2/2\,(\rho_{\mathrm{l}} - \rho_{\mathrm{v}})\, gd^2, \tag{3}$$

where κ_l and κ_{v} are the liquid and vapour dielectric constants, respectively, $\varepsilon_{\mathrm{o}} = 8.854 \times 10^{-12}\,\mathrm{F\,m^{-1}}$ and V is the root-mean-square (rms) voltage. Note that typically $\kappa_{\mathrm{v}} \approx 1.00$. It is convenient here to define a new dimensionless modulus called the electric Bond number:

$$Be \equiv h_{\mathrm{DEP}}/d = (\kappa_{\mathrm{l}} - \kappa_{\mathrm{v}})\, \varepsilon_{\mathrm{o}} V^2/2\,(\rho_{\mathrm{l}} - \rho_{\mathrm{v}})\, gd^3. \tag{4}$$

This modulus measures the strength of the DEP force compared with gravity.

It is important to realize that neither capillarity nor DEP can develop the dynamic pressure head required to pump liquid continuously from point to point. If a temperature gradient is properly imposed along the length of an electrode structure, as in the case of the dielectrophoretic heat pipe [15], liquid

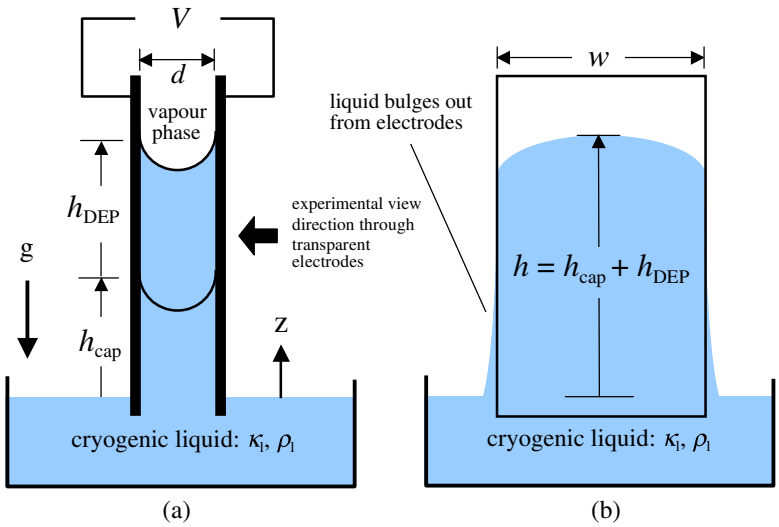

Figure 1. The parallel plate geometry. With no voltage applied to the electrodes, the capillary rise is h_{cap}. (*a*) The end-on view depicts the expected circular profile of the meniscus and the contact angle $\theta_c = 0^\circ$ which characterizes deuterium with almost all solids. When voltage is applied, the liquid rises an additional amount h_{DEP}. Unlike electrowetting, the DEP force has virtually no influence on contact angle. (*b*) The side view shows the outward bulge (exaggerated) of the liquid towards the bottom.

motion can be induced, but it is the temperature gradient that drives the motion, not the electric field. No time-average electric power is supplied to the system, just as the wick in a capillary heat pipe supplies no pumping power. It is also possible to siphon dielectric liquid between an upper and a lower reservoir using the DEP effect [16]. The electric field imposed by the electrodes maintains fluid communication between the reservoirs but, just as in a regular tube siphon, gravity establishes the pressure head that moves the liquid.

Elementary considerations reveal that the capillary and DEP contributions to the static height of rise are simply additive, so that the net measurable effect is $h = h_{cap} + h_{DEP}$. The ratio *Be/Bo* measures the relative importance of the DEP and capillary contributions:

$$\frac{Be}{Bo} = (\kappa_l - \kappa_v)\,\varepsilon_o E^2 d/4\gamma \cos\,\theta_c, \qquad (5)$$

where the rms electric field strength $E = V/d$ appears in equation (5).

Electrical breakdown in the covering gas or vapour usually imposes a limit on the maximum electric field, that is $E < E_b$. For saturated D_2 vapour at $T = 20\,K$, the breakdown field strength is $E_b \approx 2 \times 10^7\,V_{rms}\,m^{-1}$ [17]. Equation (5) teaches that, if the electric field E is limited by breakdown, the way to increase the relative importance of the DEP force is to increase κ or d, or to use a liquid possessing a larger contact angle, θ_c, or lower surface tension, γ. Assuming an electrode spacing of $d = 1\,mm$, a safety margin for the applied electric field of $E = 0.25E_b$, and using the properties of liquid D_2 at $T = 20\,K$, equation (5) gives $Be/Bo \approx 3.5$. Thus, the DEP force can be made to dominate over capillary rise.

The hydrostatic profile of the liquid along the vertical sides is difficult to calculate because it depends on hard to determine details of the shape of the sides of the plates. The vertical profile is further influenced by the strongly non-uniform electric field. In general, the liquid always bulges outwards near the bottom and recedes inwards near the top, as depicted with some exaggeration in figure 1(*b*). For cryogenic deuterium, with its low surface tension, $\gamma \approx 0.0038\,N\,m^{-1}$, and zero contact angle, $\theta_c \approx 0^\circ$, this bulging is actually minimal. The highest reach of the liquid occurs midway between the edges of the electrodes. On either side of the high point, the meniscus curves steadily down to where it becomes vertical along both edges. Prediction of the three-dimensional shape of the liquid surface at the top of the column is best done by numerical means.

5. Experiments using parallel electrodes

The experimental plates are made of glass treated with indium tin oxide (ITO), 1.1 mm thick, ~ 15 mm high and 7.6 mm wide. The ITO layer is conductive but transparent, making it possible to observe and record the shape of the liquid meniscus across the width of the electrodes. The electrode assembly is placed in a chamber connected to a cryostat, which can be cooled as low as the triple point of D_2. By carefully managing the inventory of gaseous deuterium introduced into the cryostat and controlling the temperature, we condense liquid D_2 in a pool at the bottom of the chamber. This pool serves as the reservoir depicted in figures 1(*a*) and (*b*). The viewing ports in the experimental chamber are on the top and bottom, requiring placement of a mirror inside to view the liquid rise.

Figure 2 shows the liquid rise viewed through the ITO treated glass electrodes for a range of applied voltages. It is important to note that the profile of the meniscus along the width of the electrodes does not change appreciably as the voltage is increased, indicating that the electric field has negligible influence on the curvature of the liquid/vapour surface. We gather height-of-rise data from individual digital images such as those in figure 2 by measuring the vertical

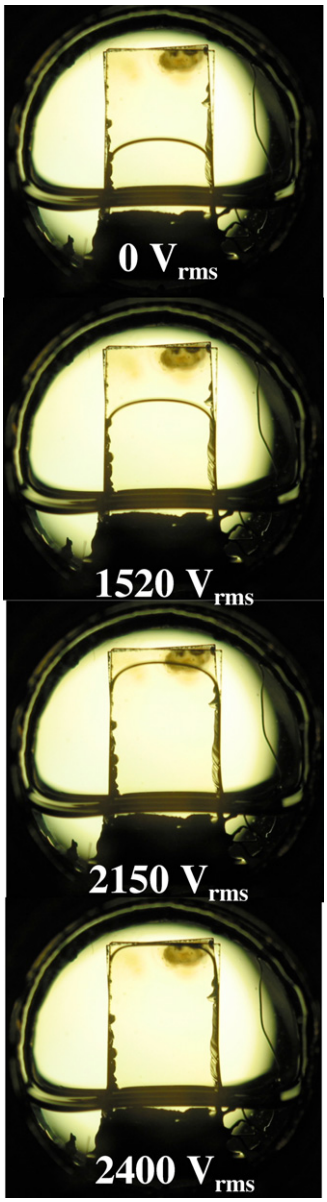

Figure 2. Meniscus of cryogenic D_2 at $T = 18.7$ K viewed through parallel, transparent ITO-coated glass electrodes, $w = 7.6$ mm, $d = 0.86\,\mu$m for 1 kHz ac voltages ranging from 0 to 2400 V_{rms}. Frequency must be high enough to avoid surface wave instabilities, but is otherwise not important.

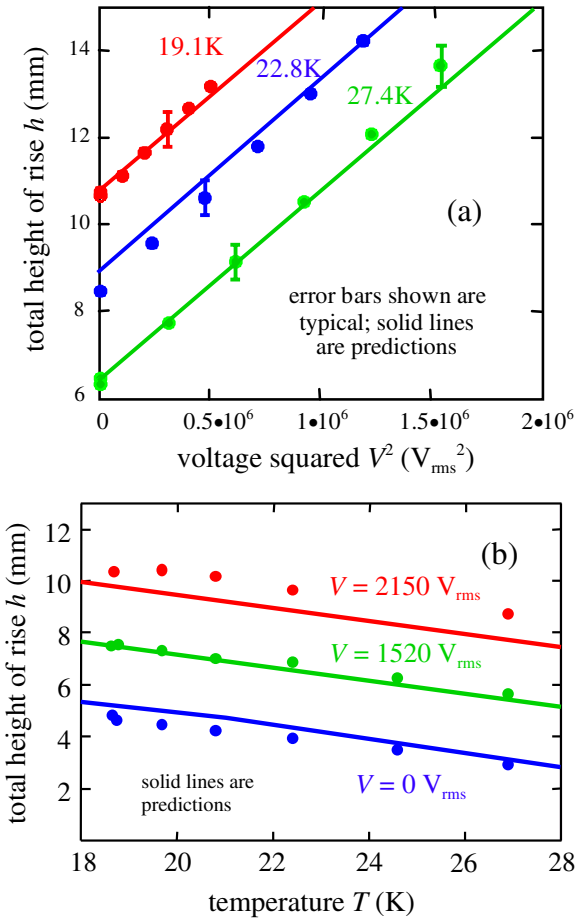

Figure 3. Height-of-rise data and predictions using $h(V) = h_{cap} + h_{DEP}(V)$ for liquid deuterium using parallel electrodes: $w = 7.6$ mm, $d = 0.43(\pm 0.02)$ mm. (*a*) h versus voltage V at various temperatures. (*b*) h versus temperature at several fixed voltages.

distance from the equilibrium level of the liquid in the pool to the highest point of the meniscus. Despite small systematic errors, due primarily to uncertainty about the exact location of the equilibrium liquid level outside the plates, these data compare quite favourably with the one-dimensional model prediction. Figure 3(*a*) plots net height-of-rise data for experiments performed at several temperatures. The solid lines in this figure are predictions for $h = h_{cap} + h_{DEP}$ based on the one-dimensional hydrostatic models used to obtain equations (1) and (3). For these curves, we employed the set of approximate, fitted temperature dependent expressions for dielectric constant $\kappa_l(T)$, liquid and vapour densities $\rho_l(T)$ and $\rho_v(T)$ and surface tension $\gamma(T)$ found in appendix A. Some of the data are obtained at temperatures lying outside the advertised range for the dielectric constant expression, but any resulting error is not expected to be significant because $\kappa_l(T)$ is a rather weak function of temperature. The error bars shown are typical.

Figure 3(*b*) plots measured height-of-rise data and predictive curves directly as a function of temperature T for several fixed voltage values. While voltage—actually the electric field magnitude $E = V/d$—does not influence the shape of the meniscus, the images in figure 4 do reveal that the temperature does have some effect. The measured radius of curvature in the plane of the electrodes at the midpoint increases from ~7 mm at $T = 18.8$ K to ~11 mm at $T = 26.9$ K, reflecting a ~45% drop in the surface tension at the higher temperature. Over this same temperature range, the density changes by only ~10%. Temperature is not believed to influence the contact angle θ_c appreciably.

One factor very critical to the success of equations (1) and (3) in predicting the net height of rise is the condition $w \gg d$, where w and d are, respectively, the plate width and spacing. In this limit, the influence of the vertical sidewalls becomes less and less significant, and the uniform electric field approximation inherent in equation (3) becomes more valid. A one-dimensional model of course cannot predict the curved

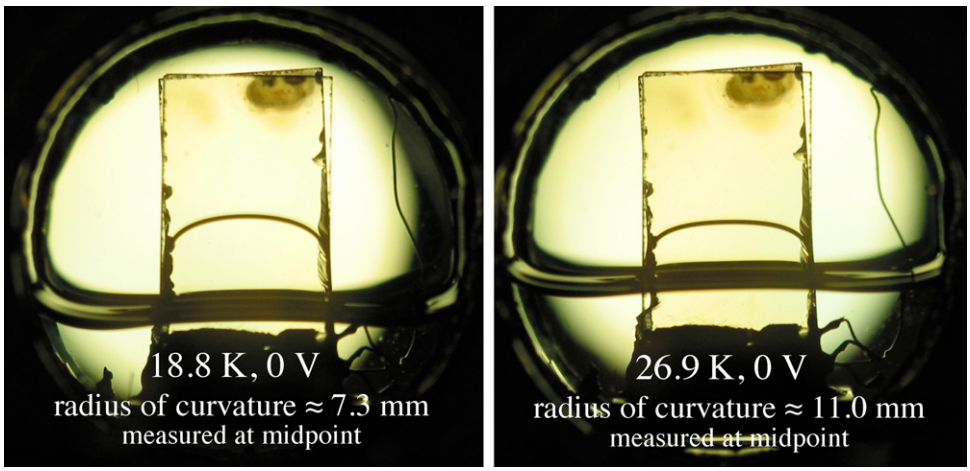

Figure 4. Effect of temperature on meniscus shape and height-of-rise h_{cap}. The temperature, but not the electric field E, affects the profile of the meniscus along the width of the electrodes through its influence on surface tension and density.

profile evident in the images of figure 2. To overcome this modelling deficiency, we used a finite element computation to solve for the three-dimensional surface between the plates. This analysis, based on a numerical energy minimization, is summarized in the next section.

6. Simulations

The significant curvature of the liquid surface parallel to the electrode plates, evident in figure 2, reveals that surface wetting can influence the maximum, measurable height-of-rise h if the plates are not sufficiently wide. For this reason, we employed the *Surface Evolver* software of Brakke [18] to solve for the shape of the liquid meniscus. This finite element tool is based on a computational algorithm that seeks the minimum energy configuration of a static liquid volume subject to wall constraints, contact angle, gravity and certain other body forces[5].

Figure 5 shows various views of the numerical solution for the meniscus of D_2 using geometric parameters representative of the actual experiment, at temperature $T = 18.7$ K and with no voltage applied. Figure 5(a) provides an oblique view of the elevated liquid between the plates and figure 5(b) shows an end-on view of the meniscus. One thing to note about the numerical solution is that the contact angle made by the liquid at the walls does not quite go to zero, presumably because of the level of mesh refinement. An enlarged view of the meniscus, shown in figure 5(c), reveals details of the actual 3D liquid surface near the top. Note that the two radii of curvature are of opposite sign. It is for this reason that the liquid height at the midpoint h_{cap} is always less than the value predicted by the one-dimensional model. Figure 5(d), the view normal to the parallel plates, is the same afforded by viewing the experiment

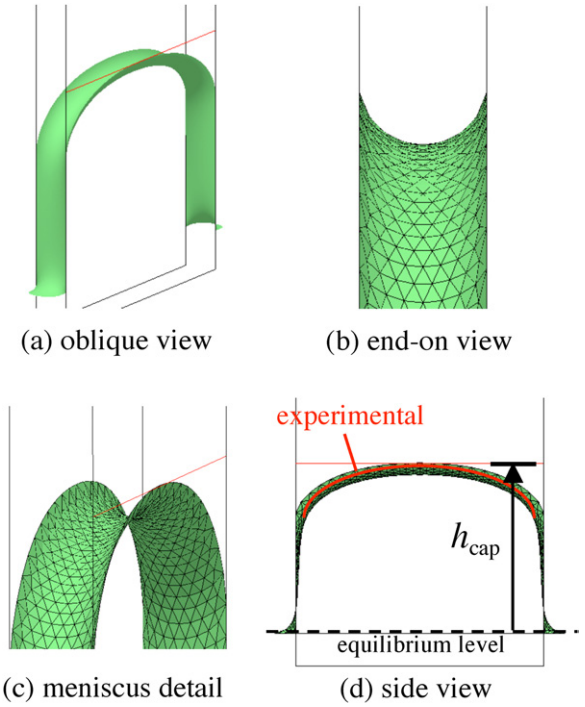

Figure 5. Numerical solution obtained using *Surface Evolver* software for the shape of the liquid meniscus between parallel plates for $w = 7.6$ mm, $d = 0.86$ mm and $T = 18.7$ K. (a) Oblique view. (b) End-on view showing the contact angle $\theta_c \approx 0^\circ$. (c) Close-up of the meniscus. (d) Side view, perpendicular to parallel plates, with superimposed profile obtained from experiment. h_{cap} is the height of rise calculated from equation (1).

through the transparent ITO glass plates. A curve fitted to an experimental image of the actual meniscus is superimposed for comparison. Correspondence is reasonably good, except very close to the vertical edges of the plates, where the actual location and configuration of the contact line cannot in fact be modelled with any confidence. The height-of-rise h_{cap} calculated from the one-dimensional model, equation (1), is also indicated in figure 5(d).

To investigate in greater detail the influence of plate width w upon the profile of the liquid deuterium meniscus and

[5] The Surface Evolver accommodates any body force that can be transformed into a surface or line force using the divergence theorem. In principle, electrical forces can be handled in this fashion; however, solution for the electric field on each facet of the mesh becomes necessary. Convergence then involves solving a tightly coupled problem where the mesh and the highly non-uniform electric field influence one another, that is both electric field and surface shape must be solved simultaneously. Surface Evolver is not designed to do this.

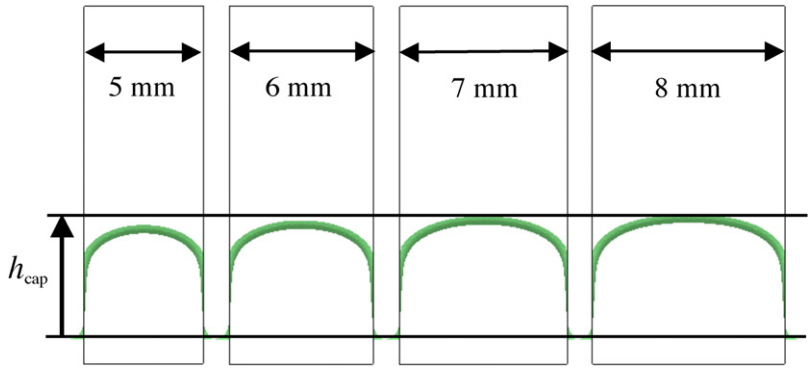

Figure 6. Side view of liquid D_2 meniscus profile between plates of spacing $d = 0.86$ mm at $T = 18.7$ K calculated using *Surface Evolver* for different values of the plate width: $w = 5$, 6, 7 and 8 mm. The top of the liquid column does not reach h_{cap}, the value predicted by the one-dimensional model, equation (1), unless $w \geqslant 7$ mm. This result may be expected to scale directly with plate spacing d.

the height-of-rise h_{cap}, we performed additional simulations using Surface Evolver. Again here, the DEP effect was not incorporated into the model. These results, shown in side view only, are provided in figure 6. Note that, as the width is increased, the maximum height of the meniscus at the midpoint approaches h_{cap}, as predicted by equation (1). For the plate spacing value used in the calculation, that is $d = 0.86$ mm, this condition is reached at $w \approx 7$ mm. For larger values of w, the meniscus exhibits a virtually flat section in the middle. It is evident, both from experiment and from the simulations supporting them, that the influence of the vertical sidewalls upon the profile can be significant.

7. Experiments using converging electrodes

The electrohydrostatic behaviour of dielectric liquids becomes more interesting when the electrodes are made to converge towards the top, as shown in figure 7(*a*). If the ratio of the spacing at the bottom and the top, b/a, is large enough, the liquid column exhibits a bifurcation. This phenomenon was first observed with conventional, room temperature dielectric liquids. If the electrodes are planar, the relationship of the height-of-rise h to the applied voltage V takes the form of a cubic polynomial as long as $a \neq b$. This equation is obtained using the Maxwell stress tensor and hydrostatic pressure balance to account for the upward DEP force, under the assumption $a < b \ll w$ [19]:

$$\underline{h}^3 - 2\underline{h}^2 + (1 + Bo)\,\underline{h} - (Bo + Be) = 0, \qquad (6)$$

where $h = \alpha h/b$ is the normalized height of rise, a and b are the plate spacings at the top and bottom, respectively, H is the electrode height and $\alpha = (b - a)/H$. Usually $H \gg w$, so that α is approximately equal to the angle between the plates in radians. For convenience, equation (6) employs modified definitions for the Bond numbers given below.

$$Bo = 2\alpha\gamma \cos\theta/(\rho_l - \rho_v)\, g b^2 \qquad \text{and}$$
$$Be = \alpha\,(\kappa_l - \kappa_v)\,\varepsilon_o V^2/2\,(\rho_l - \rho_v)\, g b^3. \qquad (7)$$

Given the cubic nature of equation (6), the easiest way to explore the hydrostatics of the converging plate geometry is to plot V as a function of $\underline{h}$. Referring to figure 7(*b*), the point on the curve where $\mathrm{d}h/\mathrm{d}V \to \infty$, identified as (V^*, h^*), becomes an observable bifurcation of the hydrostatic equilibrium, as long as the condition $0 < h^* < H$ is met. For this case, as voltage is increased, the liquid column rises upwards steadily until, at voltage V^*, it jumps from $h = h^*$ all the way to the top of the electrodes, that is $h \to H$. Once the liquid column reaches the top and the voltage is then turned back down, according to the model, static equilibrium is lost on both vertical sides at the same point, $z = h^*$, where the liquid jump occurred, and at the same voltage, $V = V^*$. It is easily shown from pressure balance arguments that, as the voltage is being reduced, $z = h^*$ will always be the first point on both sides where hydrostatic pressure equilibrium of the free surface lapses. The surface thus collapses inwards on both sides at $z = h^*$, usually trapping liquid at the top. This trapped inventory remains near the top even when the voltage is reduced to zero, probably due to contact angle hysteresis. While this behaviour occurs just as predicted in the case of room temperature dielectrics [19], experiments using cryogenic D_2 yield differences probably due to its perfect wetting property.

Figures 8 and 9, respectively, show images from an experiment performed using liquid deuterium with the voltage first monotonically increased to some $V > V^*$, and then decreased. For increasing voltage (figure 8), the column rises steadily until, at a voltage value between 1590 and 1599 V_{rms}, it jumps the rest of the way to the top, just as predicted by the one-dimensional model. On the other hand, when the voltage is then reduced (figure 9), the surface does not fully collapse at $z = h^*$, but instead forms a neck that becomes narrower and narrower as V is reduced below V^*. Eventually, the neck does rupture, but our observation is that the volume of liquid trapped near the top is neither well-controlled nor very reproducible. Data obtained from this experiment are plotted in figure 10, along with the prediction from equation (6). For rising voltage, the model predicts the column height h with reasonable accuracy; the discrepancies are almost certainly due to (i) uncertainties in the values for a and b, which must be measured before the fixture is cooled down and (ii) a slight misalignment of the plates. A clear manifestation of this misalignment is the evident asymmetry of the meniscus profile that increases as voltage is raised. The data plotted in figure 10 for reducing voltage are in two groups. The data marked by

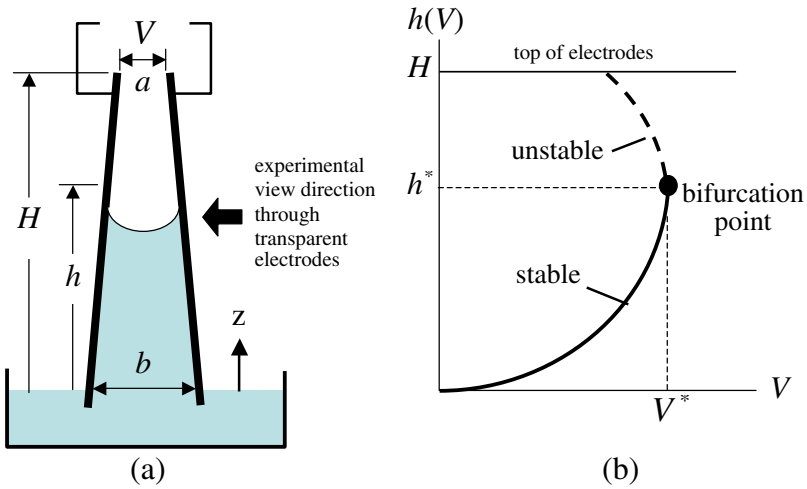

Figure 7. The converging plate experiment. (*a*) Side view of electrode geometry with definitions of parameters. (*b*) Representative $h(V)$ curve with bifurcation point at (V^*, h^*). Bifurcation is experimentally observable only if the electrode height H exceeds the critical value, that is $H > h^*$.

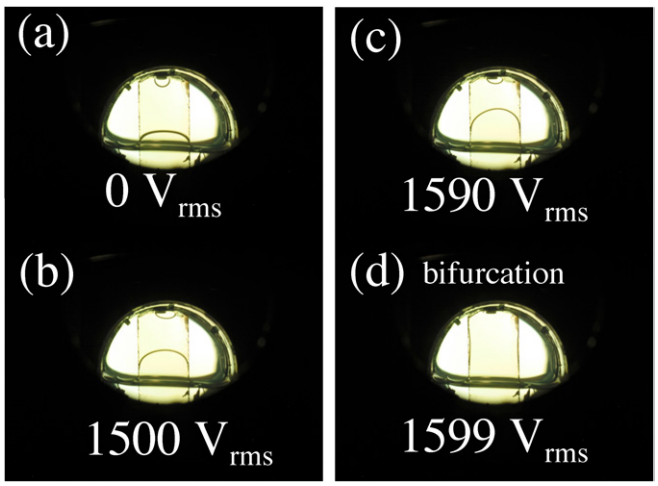

Figure 8. Meniscus of cryogenic D_2 at 23.9 K viewed through transparent, slightly convergent ITO glass electrodes, $w = 7.6$ mm, $H = 12$ mm, $a = 0.42$ mm, $b = 1.41$ mm, for increasing ac voltages at 1 kHz. The small droplet visible at the top was trapped in a previous experiment. (*a*) $V = 0\,V_{rms}$; (*b*) $V = 1500\,V_{rms}$; (*c*) $V = 1590\,V_{rms}$, meniscus approaching bifurcation point h^*; (*d*) $V = 1599\,V_{rms}$, liquid has jumped to the top.

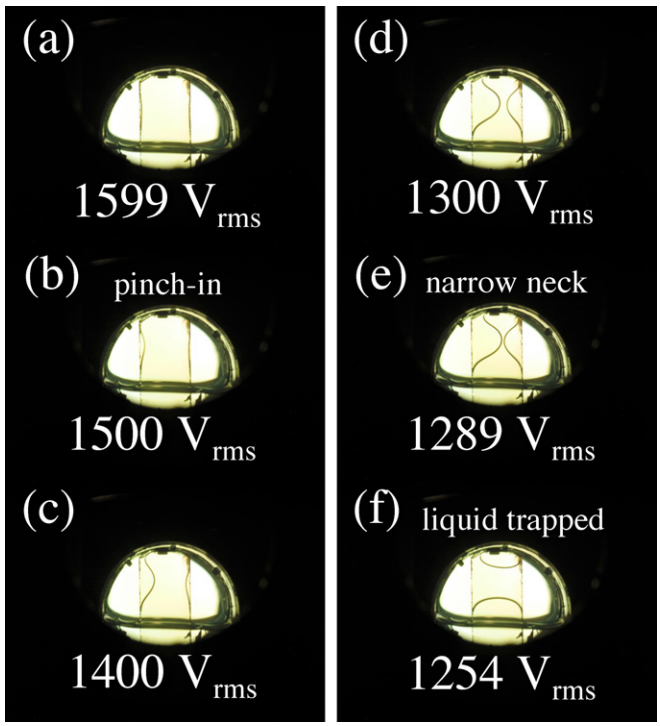

Figure 9. Meniscus of cryogenic D_2 at 23.9 K viewed through transparent, slightly convergent ITO glass electrodes, $w = 7.6$ mm, $H = 12.0$ mm, $a = 0.42$ mm, $b = 1.41$ μm, for decreasing ac voltages at 1 kHz. (*a*) $V = 1599\,V_{rms}$; (*b*) $V = 1500\,V_{rms}$, surface starting to collapse inwards; (*c*) $V = 1400\,V_{rms}$, further collapsed; (*d*) $V = 1300\,V_{rms}$, further collapsed; (*e*) $V = 1289\,V_{rms}$, only a narrow neck remains; (*f*) $V = 1254\,V_{rms}$, neck has ruptured and liquid is trapped at the top.

(×), indicating the locations of the narrowest point of the stable liquid neck shown in figures 9(*b*)–(*e*), correlate reasonably well with the calculated value of h^*. The squares (■), indicating measured column height values after the neck has ruptured, closely follow the cubic relation, equation (6).

In the experiment shown in figures 8 and 9, the plates were maintained in position by a small plastic spacer positioned at the top in the middle. This spacer has the effect of retaining some of the liquid at the top, even when the voltage is reduced to zero. Without this spacer, the trapped liquid always seems to fall. Such behaviour is unlike the highly repeatable trapping phenomenon observed with room temperature dielectrics [19], where it may be that wetting hysteresis assists in holding the trapped liquid when the voltage is removed.

8. Discussion

The bifurcation behaviour of liquid D_2 differs from the prediction based on the one-dimensional model and also from experiments with room temperature dielectric liquids, but

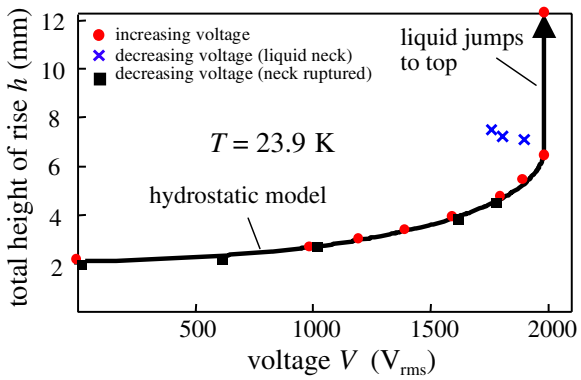

Figure 10. Experimental data and predicted $h(V)$ curve from equation (6) for converging plates, $w = 7.6$ mm, $H = 12$ mm, $a = 0.42\,\mu$m, $b = 1.41\,\mu$m. The data obtained for increasing voltage (●) match the prediction very well. For decreasing voltage, data indicated by (×) indicate the location along the vertical sides where the interface is collapsed inwards the most. The squares (■) denote the height of the column after the neck has ruptured.

only when the voltage is reduced towards V^* from values above it. The cause of this discrepancy seems to be the very low contact angle that cryogenic deuterium exhibits against the ITO glass coated electrodes. In contrast, the contact angles for the dielectric liquids used in earlier experiments conducted at room temperature were in the range from ∼70° to ∼90° [19]. When $\theta_c \approx 0°$, a thin, remarkably stable filament of liquid persists between the two plates, probably because its concave inter-electrode profile makes it energetically favourable. Equation (6) fails to predict the observed behaviour for lowering voltage because the existence (and stability) of such filaments is not accounted for in the one-dimensional, hydrostatic model. The data in figure 10 do suggest that surface equilibrium starts to fail near $z = h^*$ as we would expect, irrespective of the formation of the filament.

One major question about the use of DEP in laser target fuelling is not addressed here, namely, that the liquid fuel for laser targets will necessarily contain liquid tritium, which is highly radioactive. The energetic electrons (β particles) emitted by tritium decay introduce space charge to the liquid bulk, rendering the liquid effectively conductive, though probably not ohmic in nature. One hypothesis is that the small currents detected to flow in liquid D_2 when an electric field is applied are actually due to very small but unavoidable levels of tritium contamination [20, 21]. If there is sufficient tritium present, the mobile charges may cause the liquid to behave as an electrical conductor. In that case, the DEP mechanism will become inoperative; however, it could still be possible to actuate the liquid electrically by exploiting the electrowetting mechanism. To do so, it is necessary to coat the electrodes with a thin dielectric layer. Electrowetting has been intensively studied and is demonstrated to be very effective in the transport and manipulation of many room temperature liquids ranging from DI water to liquid mercury [22]. An investigation of the electrowetting behaviour in liquid DT would be an interesting if challenging experimental undertaking.

9. Conclusion

A simple, one-dimensional hydrostatic model for the behaviour of liquid deuterium between parallel plates under combined capillarity and liquid dielectrophoresis successfully predicts the height of rise as long as the plates are sufficiently wide compared with their spacing, that is $w/d >\sim 8$. The capillary and DEP effects are additive: $h = h_{cap} + h_{DEP}$. The actual three-dimensional meniscus shape is predicted with reasonable accuracy using the Surface Evolver tool, which seeks a numerical solution using finite elements and surface energy minimization. If the plates are made to converge towards the top, the hydrostatic equilibrium includes a bifurcation effect that manifests itself when the ratio of the electrode separation at the bottom and the top (b/a) is large enough. This bifurcation might be used to trap liquid; however, at present the reproducibility of the trapped volume for liquid D_2 is poor because of the formation of a highly stable liquid filament, which forms because cryogenic deuterium perfectly wets the plates. Precise metering of cryogenic liquids using the bifurcation effect may not be possible unless this phenomenon can be avoided.

Acknowledgments

The hydrostatic simulations were performed using the Surface Evolver software, which is freely available from K Brakke of Susquehanna University, Selinsgrove, PA (USA), at www.susqu.edu/brakke/evolver/evolver.html. This research is supported by the Office of Inertial Confinement Fusion of the Department of Energy (Cooperative Agreement #DE-FC52-08NA28302), the Laboratory for Laser Energetics at the University of Rochester and the New York State Energy Research and Development Authority. Additional support for K Kentch from Eastman Kodak Company is gratefully acknowledged.

Appendix: Temperature dependent properties of liquid D_2

For convenience, empirical relations for the temperature dependences of the relevant liquid deuterium properties are provided below. SI units are used and the temperature T is in kelvin.

Liquid mass density in kg m^{-3} (curve fit based on [10, p 62]):

$$\rho_l(T) = -0.005231T^3 + 0.3119T^2 - 8.225T + 252.9, \quad 18.7\,\text{K} \leqslant T \leqslant 35\,\text{K}. \tag{A1}$$

Saturated vapour mass density in kg m^{-3} (curve fit based on [10, p 57]):

$$\rho_v(T) = 2.03 \times 10^{-7} \times 10^{[0.5671T - 0.01508T^2 + 0.000156T^3]}, \quad 18.7\,\text{K} < T < 35\,\text{K}. \tag{A2}$$

Liquid–vapour surface tension in N m^{-1} (curve fit based on [10, p 64]):

$$\gamma(T) = 1.759 \times 10^{-7}T^3 - 1.356 \cdot 10^{-5}T^2 + 1.296 \times 10^{-4}T + 4.986 \times 10^{-3}, \quad 18.7\,\text{K} \leqslant T \leqslant 37\,\text{K}. \tag{A3}$$

Liquid dielectric constant (curve fit based on data [20]):

$$\kappa_1(T) = 1.361 - 0.00403T, \quad 20\,\mathrm{K} \leqslant T \leqslant 23\,\mathrm{K}. \qquad \text{(A4)}$$

Cryogenic deuterium perfectly wets most solids, in other words, $\theta_c = 0^\circ$ [11]. Known exceptions exist for liquid D_2 in contact with pure Cs and Rb [23].

References

[1] Melcher J R, Hurwitz M and Fax R G 1969 Dielectrophoretic liquid expulsion *J. Spacecr. Rockets* **6** 961–7

[2] Suda Y, Itoh M, Sakai Y, Matsuura K, Honma N and Kimura T 1996 Behaviour of liquid nitrogen between electrodes in a microgravity environment *Cryogenics* **36** 567–71

[3] McKenty P W, Goncharov V N, Town R P J, Skupsky S, Betti R and McCrory R L 2001 Analysis of a direct-drive ignition capsule designed for the National Ignition Facility *Phys. Plasmas* **8** 2315–22

[4] Collins T J B, Marozas J A, Betti R, Harding D R, McKenty P W, Padha P B, Skupsky S, Goncharov V N, Knauer J P and McCrory R L 2007 One-megajoule, wetted-foam target-design performance for the National Ignition Facility *Phys. Plasmas* **14** 056308

[5] Tillack M S, Goodin D T, Alexander N B, Petzoldt R W, Raffray A R, Schroen D, Sethian J D and Streit J 2003 *20th IEEE/NPSS Symp. on Fusion Energy (San Diego, CA, October 2003)* pp 624–7

[6] Sethian J D, Latkowski J, Blanchard J P, Snead L, Renk T J and Sharafat S 2005 An overview of the development of the first wall and other principal components of a laser fusion power plant *J. Nucl. Mater.* **347** 161–77
Sethian J D *et al* 2003 Fusion energy with lasers, direct drive targets and dry wall chambers *Nucl. Fusion* **43** 1693–709

[7] Harding D R, Jones T B, Bei Z, Edgell D and Chen S H 2008 Cryogenic-DT-foam targets: the new frontier *18th Target Fabrication Meeting (Lake Tahoe, CA)*

[8] Harding D R *et al* 2005 Producing cryogenic deuterium targets for experiment on Omega *Fusion Sci. Technol.* **48** 1299–306

[9] Zimmermann H, Katsen A D, Ihmig F R, Durst C H P, Shirley S G and Fuhr G R 2004 First steps on an interdisciplinary approach towards miniaturized cyropreservation of cellular nanotechnology *IEEE Proc. Nanobiotechnol.* **151** 134–8

[10] Souers P C 1986 Hydrogen properties for fusion energy (Berkeley, CA: University of California Press) chapter 5

[11] Good J and Ferry G V 1962 The wetting of solids by liquid hydrogen *Adv. Cryog. Eng.* **8** 306–10

[12] Dreyer M, Delgado A and Rath H-J 1994 Capillary rise of liquid between parallel plates under microgravity *J. Colloid Interface Sci.* **163** 158–68

[13] Pellat H 1895 Mesure de la force agissant sur les diélectriques liquides non électrisés placés dans un champ élitrique *C. R. Acad. Sci. Paris* **119** 691–4

[14] Jones T B and Melcher J R 1973 Dynamics of electromechanical flow structures *Phys. Fluids* **16** 393–400

[15] Jones T B 1974 An electrohydrodynamic heat pipe *Mech. Eng. (ASME)* **96** 27–32

[16] Jones T B, Perry M P and Melcher J R 1971 *Dielectr. Siphons Sci.* **174** 1232–3

[17] Mathes K N 1963 Electrical insulation at cryogenic temperatures *Electro-Technol.* **72** 72–77

[18] Brakke K, Susquehanna University, Selinsgrove, PA (USA), *Surface Evolver* software, available from www.susqu.edu/brakke/evolver/evolver.html

[19] Jones T B 1974 Hydrostatics and steady dynamics of spatially varying electromechanical flow structures *J. Appl. Phys.* **45** 1487–91

[20] Willis W L 1966 Electrical conductivity of some cryogenic fluids *Cryogenics* **6** 279–84

[21] Souers P C, Fearon E M, Iwamiya J H, Roberts P E and Tsugawa R T 1980 Dielectric constant and electrical conductivity of liquid D–T *Cryogenics* **20** 247–51

[22] Lee J and C-J Kim 2000 Surface-tension driven microactuation based on continuous electrowetting *J. Microelectromech. Syst.* **9** 171–80

[23] Ross D, Taborek P and Rutledge J E 1998 Wetting behavior of H_2 on cesium *Phys. Rev.* B **58** R4274–6